RESEARCH ARTICLE

Sedimentary Evolution and Controlling Mechanisms of Fluvial–lacustrine Systems in the Triassic Halahatang Formation, Tahe Oilfield, Tarim Basin, China

Qihang Ren[1], Jinhua Liu[1,*], Hongtao Ma[2], Wenpin Li[2], Xindong Diao[2] and Weili Gu[2]

[1] School of Geoscience and Technology, Southwest Petroleum University, Chengdu 610500, China
[2] Research Institute of Exploration and Development, Northwest Oilfield Company, Sinopec, Urumqi 830011, China

Abstract

The Triassic Halahatang Formation in the Tahe Oilfield, Tarim Basin, records a complex transition from fluvial to lacustrine depositional systems, yet its depositional architecture, evolutionary process, and controlling mechanisms remain insufficiently constrained. In this study, core observations, thin-section analysis, well-log interpretation, seismic attributes, heavy-mineral assemblages, palynological data, paleotopographic restoration, and sequence stratigraphic analysis were integrated to clarify sedimentary facies types, provenance directions, sandbody stacking patterns, and depositional evolution. The study area developed braided river, meandering river, and shore–shallow lacustrine systems. During deposition of the lower First Member, abundant sediment supply from the north, steep paleoslope, low base level, and strong hydrodynamic conditions promoted thick, vertically stacked braided-channel sandbodies. In the upper First Member, rising base level, reduced sediment supply, decreased paleoslope gradient, and climatic fluctuation drove a progressive transition to meandering rivers, forming thinner channel sandbodies with improved lateral continuity. During Second Member deposition, continued base-level rise and weakened fluvial energy resulted in widespread shore–shallow lacustrine deposits dominated by mud-rich sediments with locally developed sand bars and flats. The braided-to-meandering transition reflects tectonic–climatic coupling, controlled primarily by base-level rise, sediment-supply reduction, paleoslope decrease, and paleoclimate change. The proposed depositional evolution model provides an improved framework for predicting sandbody distribution and guiding hydrocarbon exploration in the Triassic clastic succession of the Tahe Oilfield.

Keywords: halahatang formation, tahe oilfield, sedimentary evolution, braided river, meandering river, shore–shallow lacustrine deposits, controlling factors.

1 Introduction

The Tahe Oilfield is the largest marine carbonate oilfield in the Tarim Basin to date, and its

Submitted: 11 April 2026
Accepted: 09 June 2026
Published: 15 June 2026

Vol. 2, **No.** 3, 2026.
10.62762/JGEE.2026.916754

***Corresponding author:**
✉ Jinhua Liu
499504140@qq.com

Citation
Ren, Q., Liu, J., Ma, H., Li, W., Diao, X., & Gu, W. (2026). Sedimentary Evolution and Controlling Mechanisms of Fluvial–lacustrine Systems in the Triassic Halahatang Formation, Tahe Oilfield, Tarim Basin, China. *Journal of Geo-Energy and Environment*, 2(3), 203–218.

sedimentary evolution and development have attracted considerable attention [1–3]. During the lowstand period, the low base level and abundant sediment supply from northern source areas promoted the development of braided river delta systems within the Halahatang Formation. Mutual erosion and stacking among braided channels formed thick lowstand sand bodies. The Triassic strata are notably marked by thick braided river delta front deposits. During the subsequent lacustrine transgression, lake water intruded from the southwest. In the highstand period, the base level rose and provenance supply weakened, resulting in the widespread development of semi-deep to deep lacustrine and shore–shallow lacustrine deposits.

In general, braided and meandering rivers are distinct fluvial morphologies resulting from different river patterns, and the transition between them is controlled by various factors. Wu et al. [4] documented the tectonic switch from Triassic contraction to Jurassic–Cretaceous extension in the western Tarim Basin, demonstrating that thrust-induced uplift along the basin margin during the Triassic enhanced sediment supply and provided the tectonic–sedimentary dynamic basis for the development of thick lowstand sand bodies in the Halahatang Formation of Tahe. Jolivet et al. [5] documented the Mesozoic and Cenozoic tectonic reactivation history of the central Tian Shan, demonstrating that compressional episodes along the northern margin of the Tarim Basin during the Triassic contributed to differential uplift and systematically influenced the provenance system supplying sediments to the Halahatang Formation. The Triassic paleogeographic reconstruction of the eastern Tethys domain [6] places the Tarim Block within a tropical to subtropical latitudinal belt, providing the paleogeographic context for inferring a semi-arid climate in the Triassic Tarim Basin, where strongly seasonal precipitation enhanced the scouring capacity of braided rivers and, together with base-level cyclicity, controlled the climatic-sequence stratigraphic coupling mechanism of the braided-meandering river transition in the Halahatang Formation. Prior studies on river pattern superimposition in similar tectonic settings [7] provide additional context for the depositional transition described here. Kasse et al. [8] proposed that the combination of rising base level, reduced sediment supply, and increased vegetation cover triggered the transition from braided to meandering rivers. Sharma et al. [9] argued that a decrease in sediment discharge and fining of sediment load are key factors in river pattern transition: during lowstand periods, high discharge and coarse-grained sediment favor braided rivers (thick stacked sand bodies). Based on data analysis from the study area and synthesis of previous research on sedimentology and provenance [10–15], this study demonstrates that the transition from braided to meandering rivers occurred over a relatively short geological time interval in the study area, thereby refining the sedimentary evolution model and identifying the controlling factors of this transition.

2 Geological Setting

2.1 Regional Geological Setting

The Tarim Basin is the largest petroliferous basin within the interior of China, covering an area of approximately $56 \times 10^4\,\mathrm{km}^2$. It exhibits a typical rhomboidal geometry with its long axis oriented in a nearly east–west direction. The tectonic boundaries of the basin are constrained by bidirectional compressional orogenic belts—the Tianshan and the Kunlun Mountains—with the Tianshan fold-and-thrust system to the north and the West Kunlun-Altun sinistral transgression system to the south [16]. The long-term tectonic and paleogeographic evolution of the surrounding Central Asian region has further influenced the Cenozoic basin configuration of the Tarim and adjacent basins [17]. Four major basement uplift belts are developed around the basin margin: the Kuruktag Precambrian metamorphic core complex in the northeastern margin, the Kalpin thin-skinned thrust nappe belt in the northwestern margin, the Tieklik basement thrust belt in the southwestern margin, and the Altun strike-slip fault belt in the southeastern margin. These uplift belts expose metamorphic basement series formed from the Neoarchean to the Paleoproterozoic, such as amphibolite-facies gneisses and migmatites. The main body of the basin is covered by Mesozoic–Cenozoic continental siliciclastic rocks and marine carbonates. Its present-day tectonic-sedimentary framework has resulted from multi-stage plate subduction, collision, and strike-slip processes since the Neoproterozoic breakup of the Rodinia supercontinent, including the Caledonian, Hercynian, and Himalayan orogenic episodes (Figure 1).

In this study, the Halahatang Formation within the study area is subdivided into three members: the First Member of the Halahatang Formation, the Upper Mudstone Member of the First Member of the

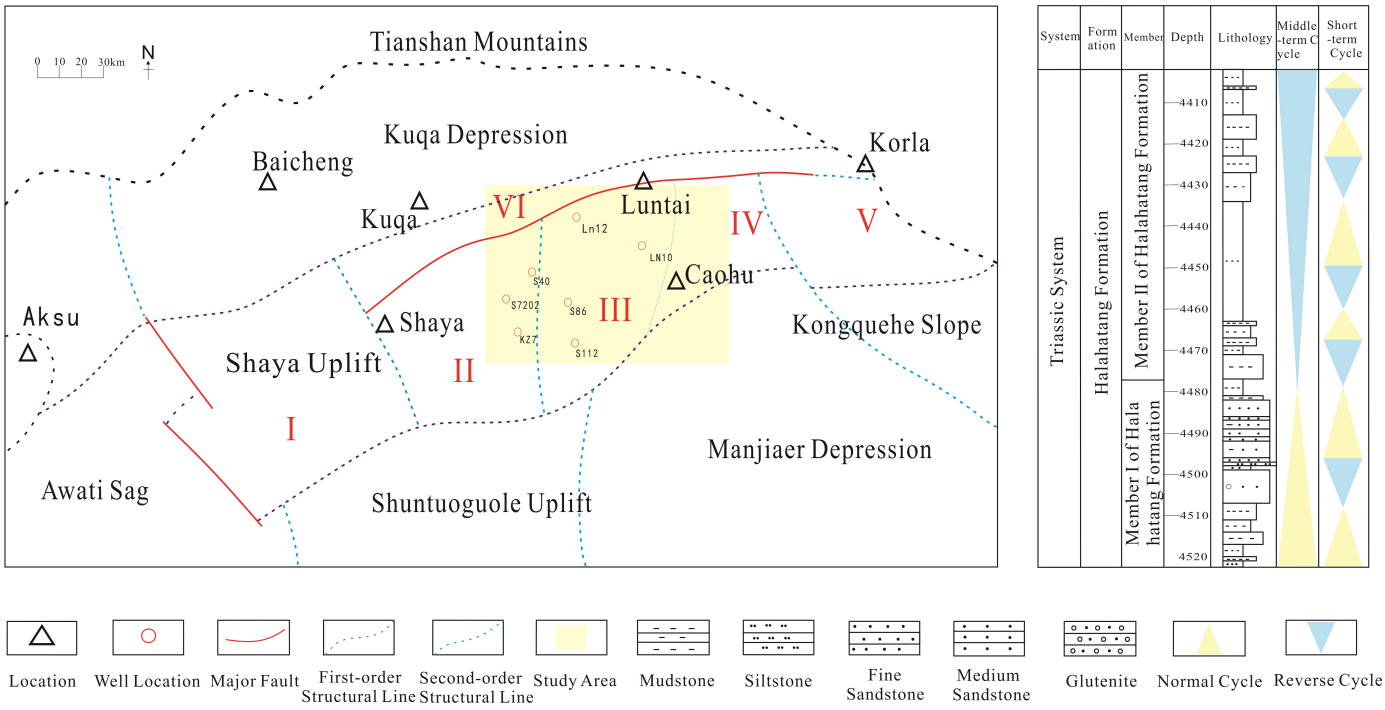

Figure 1. The location of the Triassic study area in Tahe and the comprehensive bar chart of the strata of the Halahatang Formation.

Halahatang Formation, and the Second Member of the Halahatang Formation. The study area is tectonically located in the eastern part of the Tahe Oilfield, on the southeastern slope belt of the Akekule Uplift. The Akekule Uplift initially formed as a nascent uplift during the middle to late Caledonian, manifested as a northwest-trending composite anticlinal belt with an axial length exceeding 150 km and a closure height ranging from 200 to 800 m. At the transition from the Mesozoic to the Cenozoic, regional tectonic subsidence reversal occurred, and the basin evolved from the previous fault–depression stage [18–20] into the Cenozoic retroarc foreland basin stage. During this period, the Triassic strata in the Tahe area exhibited a tectonic subsidence pattern that transitioned from an earlier "high in the north and low in the south" to a subsequent "high in the south and low in the north" configuration.

2.2 Stratigraphic Sequence Division

Influenced by the active belts along the northern and southern margins of the Tarim Plate, the sequence boundaries in the Tarim Basin do not coincide with their counterparts in the global sequence stratigraphic framework [21, 23]. The multi-stage tectonic history of the Tarim Craton, extending back to the Neoproterozoic breakup of Rodinia [22], has fundamentally shaped the inherited structural framework that continues to influence Mesozoic accommodation space dynamics and sequence development. These characteristics indicate that regional tectonic activity, by controlling accommodation space dynamics and sediment supply flux, governs the allogenic evolution of the sequence stratigraphic framework. Based on the analysis of lithological assemblage variations, sedimentary facies transition surfaces, and sedimentary structures of the Halahatang Formation in the study area, and taking into full consideration the stratigraphic development characteristics in different regions, the Triassic Halahatang Formation is divided, in terms of the stacking patterns of short-term base-level cycles, into three intermediate-term cycles (base-level rise, initial fall followed by rise, and fall) and four overall short-term cycles (rise, fall, rise, and fall).

In the upper part of the Triassic Halahatang Formation in the study area, with changes in the external sedimentary environment, the base level transitioned from falling to rising. Under the dynamic background of continuous base-level rise, controlled by the increasing A/S ratio (accommodation space / sediment supply rate) mechanism [24–27], the hydrodynamic conditions gradually shifted from being dominated by tractive currents to being dominated by suspended load. The grain size of clastic particles exhibits a vertical decreasing trend. Concurrent with the positive expansion of accommodation space and an increase in sediment

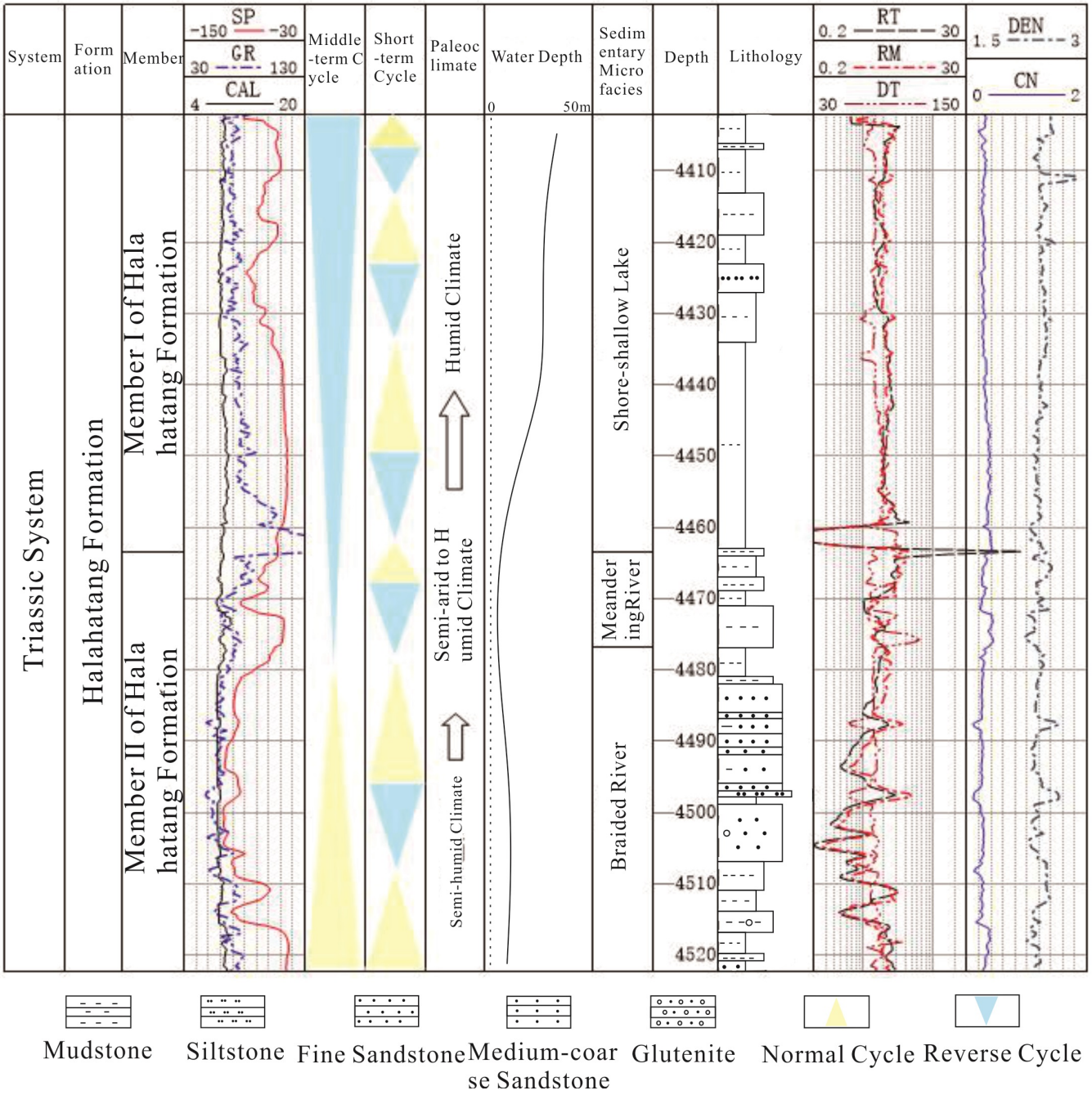

Figure 2. Comprehensive columnar diagram of the braided -meandering river conversion sedimentation in the Halahatang Formation.

accumulation rate, the sand bodies gradually thin from thick layers in high-energy environments, ultimately forming a retrogradational parasequence set (Figure 2).

3 Samples and Methods

3.1 Sample and Data Sources

The study was conducted in the central–southern Akekule Uplift, Tarim Basin, targeting the Triassic Halahatang Formation. A comprehensive dataset was collected from 25 exploration and development wells, among which 8 wells with continuous coring were selected for detailed core observation and sampling. A total of over 800 meters of core and 200 thin sections were systematically examined. Conventional well logging data, including natural gamma (GR), spontaneous potential (SP), density (DEN), acoustic (AC), and compensated neutron (CNL), were acquired for sequence stratigraphic subdivision and facies interpretation. Seismic data with a bin size of 25 m × 25 m and a dominant frequency of 25–35 m

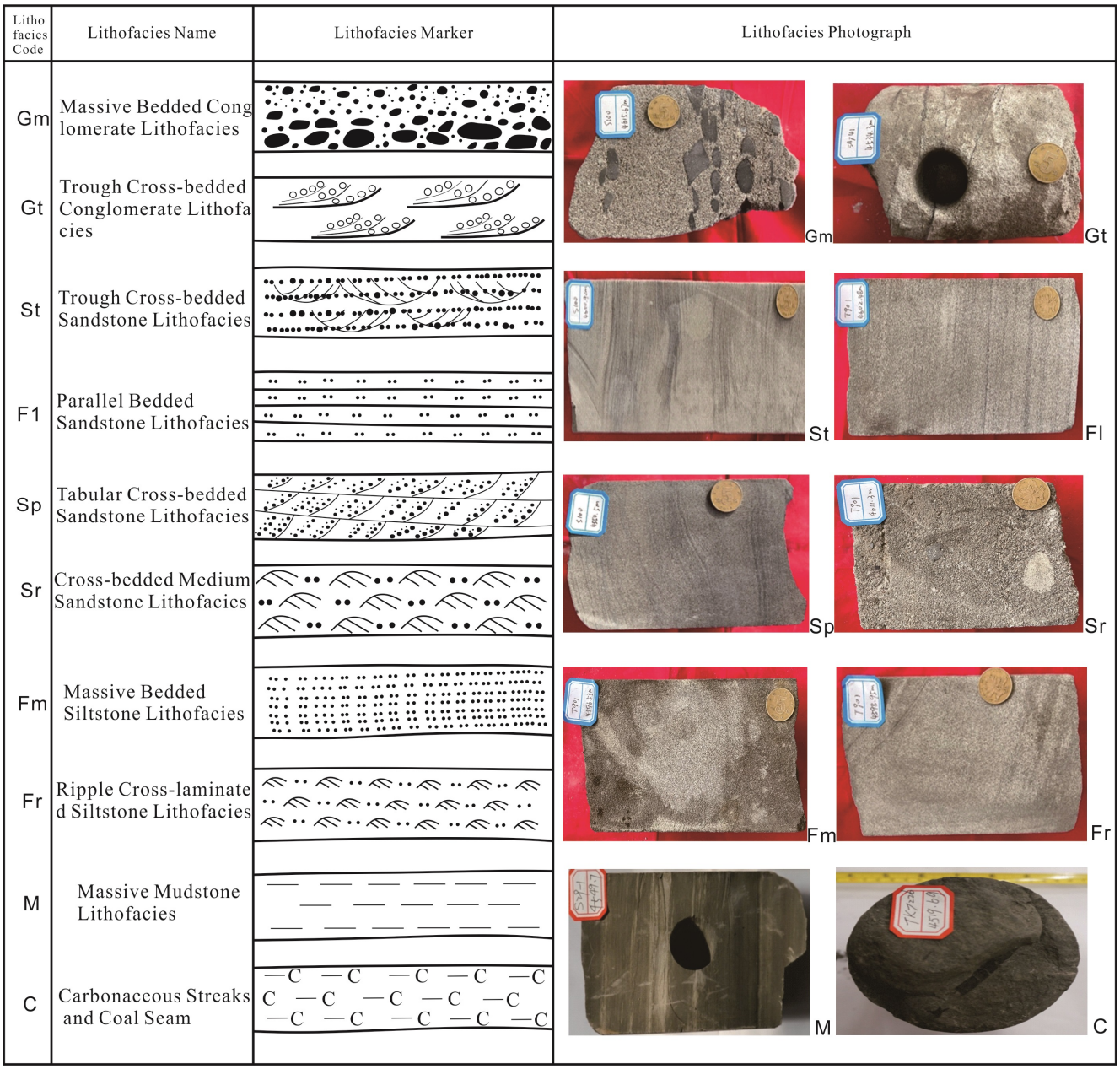

Figure 3. Typical lithofacies types of the Halahatang Formation.

were used for structural restoration and seismic facies analysis. In addition, spore-pollen and heavy mineral samples were collected from representative wells to reconstruct paleoclimate and determine provenance characteristics.

3.2 Experimental and Analytical Methods

Core observation and thin-section microscopy were performed to identify lithology, grain size, sedimentary structures, and lithofacies types. Provenance analysis was carried out by examining heavy mineral assemblages, detrital compositions, and seismic RMS amplitude attributes. Paleotopography was restored using density-log based compaction correction and paleothickness calculation, and paleoslope gradients were quantified from restored thickness and well spacing. Paleoclimate was reconstructed through spore-pollen assemblages and sediment color analysis. Sequence stratigraphic division and A/S ratio (accommodation/sediment supply) calculation were performed to analyze base-level evolution, and well-tie sections and seismic attribute slicing were integrated to characterize sandbody architecture and depositional evolution.

4 Results

Based on the integrated analysis of the Triassic sandstone thickness contour map, sandstone

percentage content, paleotectonic morphology, and grain size characteristics in the eastern part of Block 2 of the Tahe Oilfield, it is concluded that the provenance of the Triassic Halahatang Formation was exclusively from the north, including northeastern and northwestern provenance systems, while no southern provenance existed. Combined with core observations and single-well and multi-well correlation facies interpretations, the Halahatang Formation in the study area is interpreted to have developed braided river, meandering river, and shore–shallow lacustrine deposits.

4.1 Lithofacies Types

Lithofacies is the material expression of sedimentary environment and conditions. Lithofacies changes reflect variations in hydrodynamic conditions during different depositional stages and are key for analyzing sedimentary processes. Ten lithofacies types are identified in this study, including two conglomerate lithofacies, six sandstone lithofacies, and two mudstone lithofacies (Figure 3).

Massive bedding conglomerate facies (*Gm*): Affected by the strong source material from the north, the sorting is generally poor, indicated by the mixed sizes of the gravel and significant differences in rounding, reflecting the lack of hydraulic sorting during rapid near-source accumulation. The overall grain size is coarse, with a wide range of gravel sizes, and intercalated with sand or silt-sized fillers, forming thick-bedded structures, which are the products of bottom retention deposits in braided channels or underwater distributary channels.

Channelized cross-bedded conglomerate facies (*Gt*): Coarse clastics are dominant, with medium-sized gravel, moderate sorting and rounding, indicating its formation in a rapid near-source accumulation environment. The coarse clastic accumulation of the conglomerate facies and the complex layering structure correspond to the intense erosion-transportation-deposition process of braided channels during floods. The continuous scouring of the main channel flow on the base forms deep channels, which belong to the scouring deposits of underwater distributary channels in braided rivers.

Channelized cross-bedded sandstone (*St*): This sedimentary facies forms in a medium to strong hydrodynamic environment, with medium to fine sandstone as the main lithology, good sorting and rounding. Its grain sequence is the core indicator recording the dynamic evolution process of meandering rivers from vertical erosion dominance to lateral stable accretion dominance, and it is the product of meandering river migration.

Parallel bedding sandstone facies (*Fl*): In braided river environments, horizontal bedding siltstone usually develops in the low-energy environment of secondary channels or floodplains during brief still water periods; while in meandering river environments, this facies mainly develops in floodplains, floodplain swamps or the tops of point bars, which is the result of lateral and vertical accretion. Due to the stable single channel and wide floodplain of meandering rivers, the siltstone is thick and has good lateral continuity, often interbedded with massive mudstone and calcareous mudstone.

Planar cross-bedded sandstone (*Sp*): This facies is characterized by internally inclined foreset beds of medium to coarse sandstone. In the meandering river bend section, the flow is affected by centrifugal force to produce spiral motion, with the bottom flow scouring the concave bank and the surface flow carrying sediments to the convex bank and depositing them in an inclined manner. Its formation mechanism is directly related to the lateral accretion of meandering river point bars.

Wave ripple bedding medium sandstone (*Sr*): The sandstone is transported by a mixture of suspended and bedload under moderate hydrodynamic fluctuations and intermittent deposition sequences, reflecting the sedimentary dynamics of braided rivers during the alternating periods of brief stability and frequent flood events in secondary channels or marginal areas, which is the rapid migration and multi-stage superimposition of braided river migration deposits.

Massive bedding siltstone facies (*Fm*): Massive siltstone is rapidly deposited during floods or debris flows. The braided river sediments are rapidly accumulated in low-energy environments without sorting due to flood overflow, with some scouring surfaces or torn mud-gravel at the bottom and fine suspended mudstone covering the top, forming a coarse-fine sedimentary cycle.

Sand ripple cross-bedded siltstone (*Fr*): Sand ripple cross-bedded siltstone is a typical facies in meandering river sedimentary systems, with lithology of fine to medium siltstone, revealing the low to medium energy hydrodynamic conditions of meandering rivers

and the forward migration and deposition process of meandering river beds under the action of flow.

Massive mudstone facies (*M*): In braided rivers with multiple channels and high energy, massive mudstone only develops sporadically in temporarily abandoned channels or floodplain depressions, presenting isolated lens-shaped structures; while in meandering rivers with stable lateral accretion and wide floodplains, massive mudstone forms in the still water environment at the end of abandoned channels or breach fans, presenting sheet-like or thick-bedded structures, often containing plant root fossils or bioturbation structures, reflecting the combined effect of continuous suspended sedimentation and biological modification.

Carbonaceous streaked mudstone facies (*C*): The carbonaceous streaked mudstone facies is characterized by millimeter-scale alternating bands of black organic matter layers and gray mudstone, reflecting the coupling process of organic matter enrichment and clay sedimentation under periodic algal blooms, input of terrestrial plant debris or seasonal anoxic events in a still water reducing environment.

4.2 Well-tie Section

The strike of the cross-section is consistent with that of the provenance in the northwest (Figure 4). Tectonic movements resulted in relatively thick braided river deposits in the first member of the Ha Formation.

The thickness of braided-channel sandbodies in the lower part of the first member gradually decreases from west to east, and interchannel microfacies occur in the eastern area. The upper part of the first member consists of a 10–18 m thick mudstone formation intercalated with thin-bedded sandstone, within which mouth bars, floodplains, flood lakes and other microfacies are developed between riverbeds, along with two major river channels. The second member of the Ha Formation is dominated by grayish-black mudstone with local thin-bedded sand bodies and a high content of charcoal fragments. A set of carbonaceous mudstone is developed at the bottom of the second member. The overall sedimentary setting is a shore-shallow lake subfacies, including three microfacies: shore-shallow lake mud bay, shore-shallow lake sand flat, and shore-shallow lake sand bar.

4.3 Braided River

Macroscopically, controlled by strong sediment sources in the north, the first member of the Halahatang Formation is coarse-grained, with sandbody thickness ranging from 5 to 25 m, characterized by thick sandbodies intercalated with thin-bedded fine conglomerates. Sandbodies are mutually superimposed, forming braided river delta deposits with mutually incised channels [28, 29]. A small amount of gravel deposits occurs at the bottom, while the top sediments are dominated by fine sandstone, showing an overall normal cycle. The typical lithofacies sequence is (Gm-Gt-Fl-Sr-Fm-M).

Microscopically, the bottom deposits of the first member were formed in the early braided river stage, with sedimentary facies including braided river channels, lateral margins of braided channels, and interdistributary bays of braided rivers (Figure 5a). Widespread accumulation of fine conglomerates reflects proximal rapid denudation and high-energy transport. During this period, channels frequently shifted and migrated, well-developed basal scour surfaces occurred, and mud pebbles as well as imbricated gravels were common in lag deposits. As hydrodynamic energy gradually weakened, sediments gradually transitioned upward to medium-fine sandstone. Bedding structures evolved from large-scale planar cross-bedding to small-scale trough cross-bedding and horizontal bedding, and channel deposition shifted from active vertical aggradation to intermittent overbank deposition. The overall normal grading cycle records the weakening hydrodynamic process from strong scouring to weak sedimentation. Its vertical superposition pattern of sandbodies and laterally discontinuous distribution are typical responses to multi-channel interweaving and rapid migration of braided rivers.

4.4 Meandering River

Macroscopically, under the control of the base-level rising cycle, the upper sand bodies of the First Member of the Ha Formation exhibit distinct evolutionary characteristics of a meandering river depositional system. The vertical stacking pattern of sand bodies gradually transitions from thick massive sandstones of early braided rivers to thin-bedded interbedding of mud and sand. The thickness of single-stage channel sand bodies decreases to 2–5 m, with enhanced lateral continuity, showing a "rhythmic interbedding" feature of fine sandstone and silty mudstone.In terms of external geometry, channel sand

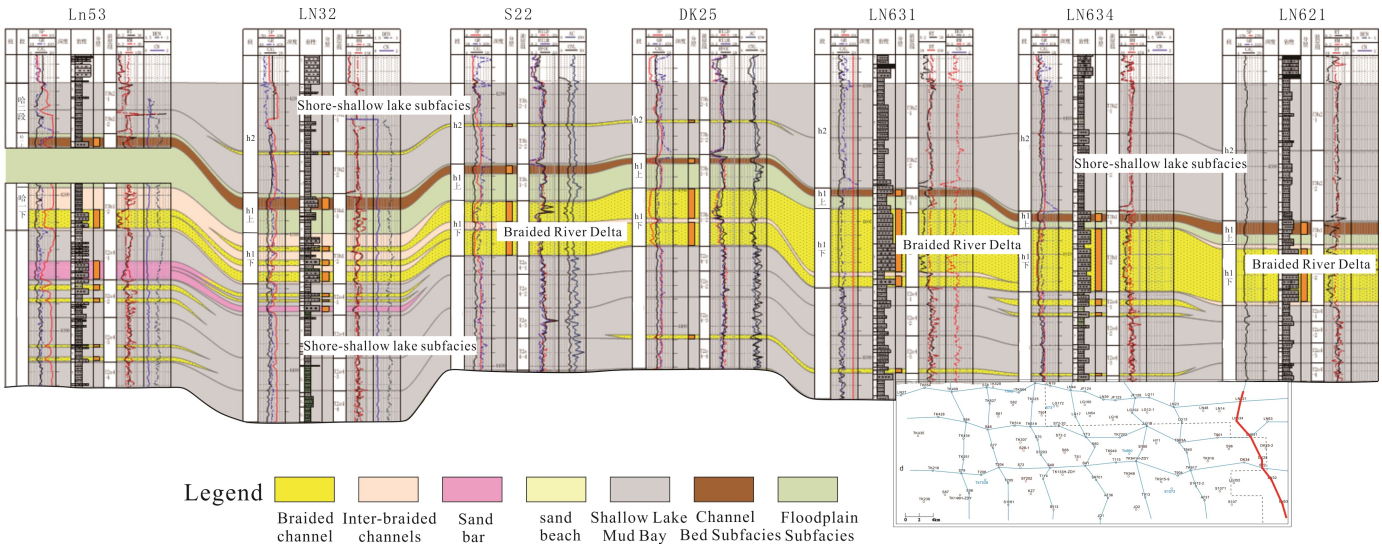

Figure 4. Characteristics of the Well-Tie Section of the Triassic Halahatang Formation in the Tahe Area (Top-Flattened) and Schematic Map of Section Strike.

bodies show a lenticular to wedge-shaped geometry. Point-bar sand bodies formed by lateral accretion are interleaved with muddy fills of abandoned channels, forming a broad "lenticular" complex consistent with the typological framework of meandering river deposits [30]. In the vertical succession, stacked sand bodies formed by multistage bend-channel migration, under the control of base-level cycles, collectively constitute a retrogradational assemblage characterized by upward-increasing mud content and decreasing sand body connectivity. The succession displays an overall dual-structural feature, with a lithofacies sequence of (St-Sp-Fr-M-C).

Microscopically, four normal cycles are identified in the upper sand bodies of the First Member of the Ha Formation, with distinct basal scour surfaces representing typical channel characteristics. In terms of grading, a typical normal grading structure is present. The base commonly shows scour surfaces and lag deposits of pebbly medium-grained sandstone, which grades upward into fine-grained sandstone and siltstone, and is capped by dark mudstone or calcareous mudstone at the top.Locally developed low-angle cross-bedding shows multi-directional intersecting foresets, intercalated with a small amount of grayish-black carbonaceous streaks (carbonaceous particle size 0.5-2 mm). Local intervals contain gravels with extremely low roundness, showing angular to subangular shapes (Figure 5b).

4.5 Shore-shallow Lacustrine

In the Second Member of the Halahatang Formation, the sedimentary facies in the study area are primarily shore-shallow lacustrine deposits, dominated by shore–shallow lacustrine mudflats. The sedimentary environment mainly consists of littoral or shallow lacustrine settings. The study area is generally characterized by abundant mud and sparse sand, reflecting a large-scale lacustrine transgression event.

Although the transgression was extensive in area, its depth was limited, resulting in the overall development of shore-shallow lacustrine deposits. In the western and central regions, however, numerous shore–shallow lacustrine sand beaches are developed, while a few discontinuous sand beaches occur in the northeastern and southern parts. A substantial amount of provenance material was transported into these areas to form deposits. The overall lateral continuity of sand bodies is relatively good. The following microfacies are developed: shore–shallow lacustrine mudflats, shore–shallow lacustrine sand beaches, and shore–shallow lacustrine sand bars (Figure 5c).

5 Discussion

5.1 Controlling Factors on Sedimentary Evolution

The upper interval of the first member of the Halahatang Formation exhibits obvious sedimentary transition characteristics of fluvial facies. Combined with analyses of sedimentary structures and sedimentary microfacies, the provenance supply, slope gradient, paleoclimate, and base-level cycle-four major influencing factors-were investigated to analyze the genetic mechanism and sedimentary characteristics of the braided river to meandering river transition in

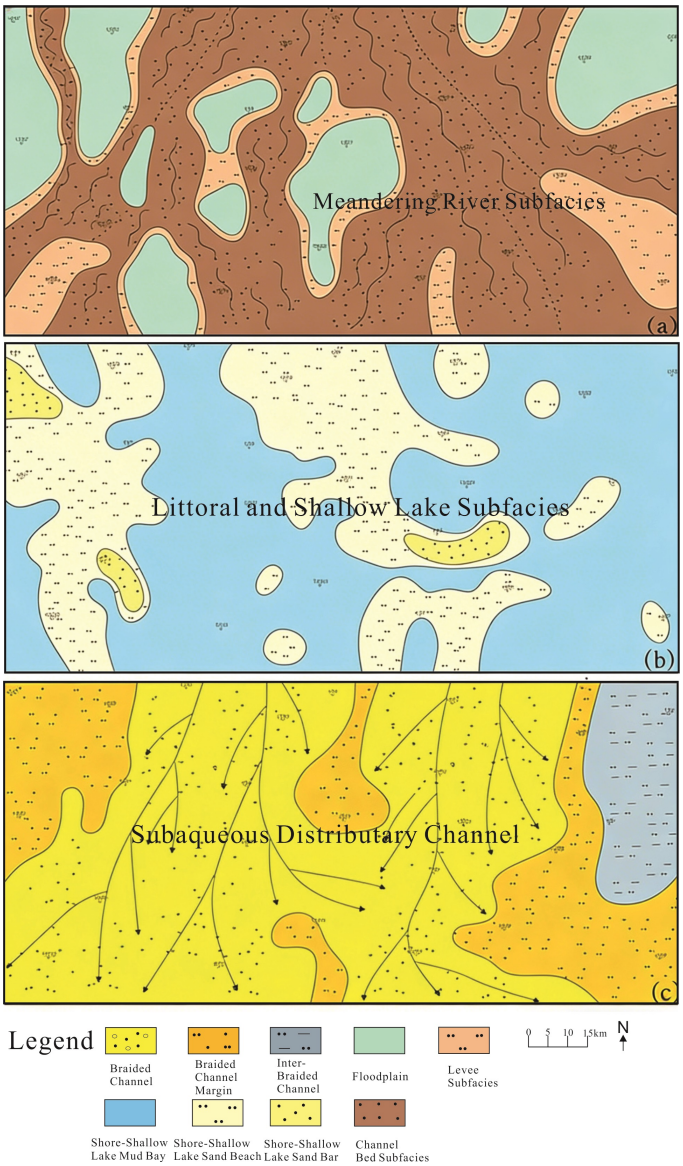

Figure 5. The sedimentary facies plan of the Halahatang Formation in the study area (sedimentary facies plan of the braided river in the first section of Halahatang (a), sedimentary facies plan of the upper curved river in the first section of Halahatang (b), sedimentary facies plan of the coastal shallow lake in the second section of Halahatang (c)).

the upper part of the first member of the Halahatang Formation. Among these, base-level change and sediment supply are considered primary drivers, whereas paleotopographic slope and paleoclimate serve as modulating factors.

5.1.1 Provenance supply and sediment input

The root-mean-square (RMS) amplitude attributes of the Halahatang Formation in the study area (Figure 6) indicate the presence of northern and northwestern provenance systems. Provenance supply gradually weakened from the upper part of the Akekule Formation to the second member of the Halahatang Formation. During the depositional period of the first member of the Halahatang Formation, provenance supply was abundant and transport distances were short, resulting in sediments dominated by coarse-grained conglomerates. The rock detrital components were complex, with low roundness and poor sorting, and braided river deposits were well developed.As the provenance supply intensity decreased to a moderate level, the sedimentary response of the first member changed significantly: braided river channel sandbodies and meandering river point-bar sandbodies were vertically superimposed, planar cross-bedding developed, sandbody thickness decreased but lateral continuity increased.By the second member of the Halahatang Formation, regional provenance supply further diminished. Sediments consisted of interbedding of siltstone, argillaceous siltstone and thin-bedded mudstone, and the depositional system fully evolved into a shore-shallow lake environment.

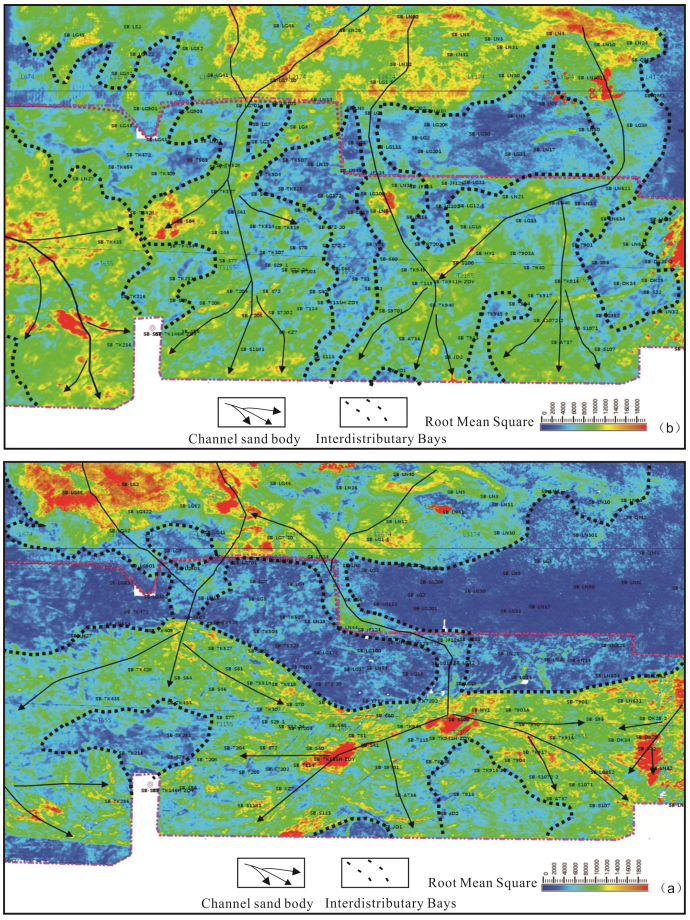

Figure 6. Root mean square amplitude attribute map of the Triassic system in the Tarim Basin of the study area (Halahatang Group (a), Akkule Group (b)).

5.1.2 *Paleotopographic Slope and Accommodation Variation*

Paleostructure restoration research can reconstruct the paleo-slope of strata, and many mature methods have been established by previous studies for sandstone intervals. Drawing on the depth-dependent compaction regularity documented in subsurface porous media studies [31], a porosity–depth function applicable to sandstone intervals is expressed as follows:

$$\Phi(z) = \Phi_r + \frac{(\Phi_0/\Phi_r)\cdot(1+\Phi_r)}{(\Phi_0-\Phi_r)+(1+2\Phi_0-\Phi_r)\cdot\exp[\gamma_g\alpha\cdot(1+\Phi_r)z]} \quad (1)$$

where $\Phi(z)$ — porosity at an arbitrary depth; Φ_0 — surface porosity; Φ_r — residual porosity; z — depth; α — a constant; $\gamma_g = (1 + 2M)$, M — the ratio of horizontal stress to vertical stress; g — acceleration due to gravity.

Since the porosity calculation formula is only applicable to reservoir formations with high porosity such as sandstone, when the same formation is buried at different depths, the internal porosity gradually decreases due to the increasing pressure from overlying strata, resulting in thinning of the formation thickness. Accordingly, the formation density also increases gradually.

The density of the target interval obtained from density logging data is used to restore formation compaction based on the law of conservation of mass. Its core relies on density logging data and sandstone percentage (Figure 7), making it suitable for mixed rock sequences and transitional lithologic formations. Based on this, Mou [32] proposed a correction formula for mixed rock formations:

$$H_0 = H \times \left[V_s \cdot \frac{\rho_{ms} - \rho_b}{\rho_{ms} - \rho_w} + (1 - V_s) \cdot \frac{\rho_{mn} - \rho_b}{\rho_{mn} - \rho_w} \right] \quad (2)$$

where H_0 — the restored formation thickness, H — the present-day formation thickness, ρ_m — the theoretical density of sandstone and mudstone, ρ_b — the bulk formation density from logging, ρ_w — the density of pore water, ρ_{ms} — the sandstone matrix density, ρ_{mn} — the mudstone matrix density, V_s — the sandstone percentage.

The calculated density (DEN) of mudstone formations at a given depth can be obtained using the above formula, and the restored formation thickness can be further calculated. In this study, the paleoslope of the Halahatang Formation in the Tarim Basin was reconstructed by calculating paleoformation thickness combined with well spacing to determine the slope gradient (Table 1).

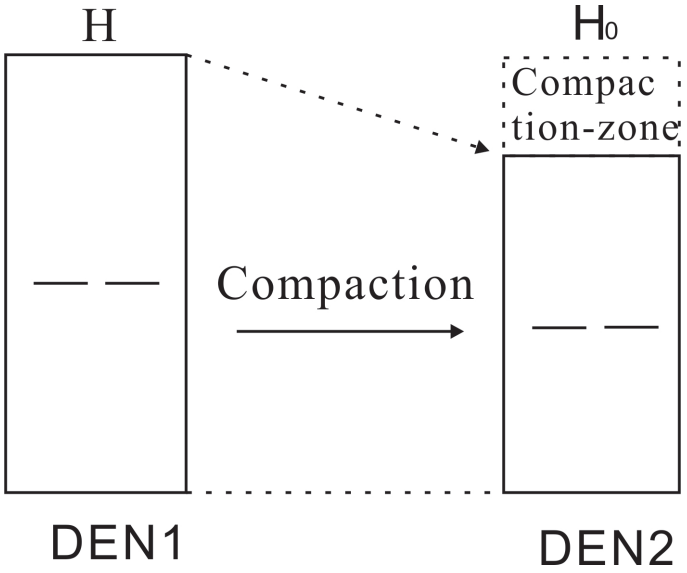

Figure 7. Compaction correction illustration.

$$\tan\alpha = \frac{H_j - H_g}{L} \quad (3)$$

where $\tan\alpha$ — paleoslope; H_j — present formation thickness; H_g — paleo-thickness; L — well spacing.

The paleogeomorphic slope in the lower part of the First Member of the Halahatang Formation reaches up to $0.93°$–$1.85°$. The paleodrainage network revealed by high-precision spectral decomposition technology is characterized by dense dendritic branching, indicating the development of a typical braided river sedimentary system under strong hydrodynamic conditions. Seismic facies show progradational reflection configurations with high amplitude and low continuity, and the paleocurrent energy index ranges from 6.8 to 7.5, representing a sedimentary model of braided rivers with "wide channels and multiple sand bars" under strong hydrodynamics.

As tectonic activity declined episodically, the paleotectonic subsidence rate in the upper part of the First Member decreased to $0.12\,\mathrm{mm/a}$, and the paleogeomorphic slope decreased to $0.42°$–$0.83°$. The channel sinuosity ranges from 1.5 to 2.3, indicating relatively stable channels with a low width-to-depth ratio (< 40), and the paleocurrent energy index

Table 1. The paleoslope of the Halahatang Formation.

Interval	Well No.	Thickness (m)			Paleo-thickness (m)	Well Spacing (km)	Paleoslope (°)
		Total	Sandstone	Mudstone			
The 2nd Member of the Ha Formation	TK216	52.37	5.32	47.05	67.83	1.76	0.51
	S79	46.83	6.82	40.01	63.25	2.41	0.39
	T208	47.24	4.25	42.99	72.18	1.82	0.78
	T204	42.12	3.24	38.88	58.21	1.46	0.63
	S72	41.32	4.72	36.60	56.91	1.24	0.72
Upper part of the 1st Member of the Ha Formation	TK216	18.12	3.20	14.92	35.21	1.76	0.55
	S79	19.86	2.19	17.67	37.65	2.41	0.42
	T208	21.18	2.08	19.10	39.02	1.82	0.56
	T204	17.62	4.95	12.67	34.12	1.46	0.64
	S72	16.52	5.32	11.20	34.58	1.24	0.83
Lower part of the 1st Member of the Ha Formation	TK216	51.25	46.32	4.93	92.83	1.76	1.31
	S79	50.16	48.65	1.51	89.21	2.41	0.93
	T208	52.37	45.24	7.13	90.14	1.82	1.23
	T204	42.73	40.82	1.91	82.17	1.46	1.55
	S72	46.82	42.21	4.61	86.93	1.24	1.85

dropped to 4.2–5.1. The vertical cycles of sand-mud ratio show periodic variations of 5–8 m. Seismic attributes display a composite architecture of "vertical aggradation and lateral migration" between braided river mid-channel bars and meandering river point bars [33], a pattern interpretable within the sequence stratigraphic framework of base-level-controlled sandbody stacking [34] (Figure 8). The channel belt width narrowed to 1.2–2 km, reflecting the transitional nature of river types under weakened hydrodynamic conditions.

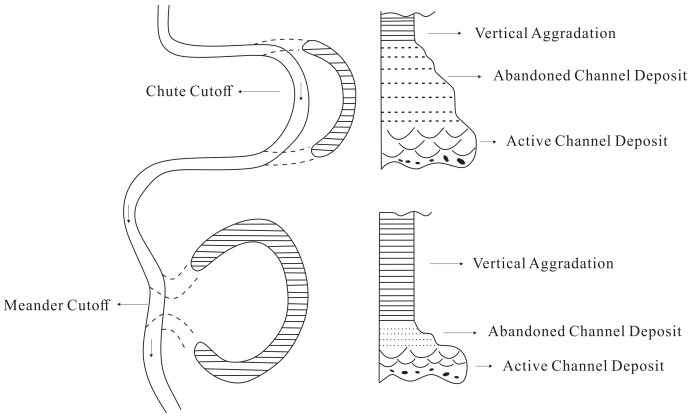

Figure 8. Sedimentary model of the meandering river channel.

By the depositional period of the 2nd Member of the Halahatang Formation, regional tectonism entered a stage of peneplanation, and the paleotopographic slope decreased to 0.39°–0.78°. Large-scale lobes prograded toward the center of the lake basin, the sand-to-strata ratio was further reduced, and sedimentary microfacies evolved into a shore-shallow lacustrine system characterized by alternating wave-controlled beach bars and sheet sands.

5.1.3 Paleoclimate evolution and hydrodynamic conditions

Spores and pollen are reproductive cells of plants with relatively stable genetic characteristics. Plants of certain genera and species produce spores and pollen of specific morphological types, so it is generally feasible to reconstruct paleovegetation and paleoclimate based on palynological data [35, 36].

Palynological study of the Halahatang Formation shows that gymnosperms are most abundant in the lower part of the First Member, dominated by Pinaceae with minor Cupressaceae, indicating a semiarid paleoclimate. Ferns reach their maximum content in the Second Member, mainly consisting of Pteris and sculptured trilete spores, suggesting that the shore-shallow lacustrine deposits of the Second Member formed under a warm and humid paleoclimate [37] (Figure 9).

In addition, plant debris alternates with purplish-red and brownish-red mudstone drapes in the sedimentary succession of the upper First Member, reflecting a paleoclimatic transition from subhumid to semiarid conditions. By the depositional period of the Second Member, mudstones are grayish-black and

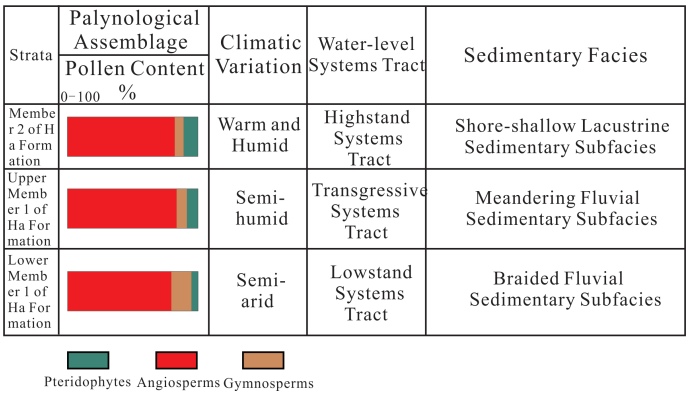

Figure 9. Spore-pollen assemblages of the Halahatang Formation.

gray, indicating a shift back to humid paleoclimatic conditions.

5.1.4 Base-level Change and A/S Ratio Control

Paleoclimatic changes have shaped the development pattern and sedimentary characteristics of fluvial systems in a stepwise manner. During the early depositional stage of the First Member of the Halahatang Formation, the regional climate was dominated by persistently humid conditions. Abundant precipitation and stable runoff provided the hydrodynamic foundation for the development of a braided river system. Under a humid climate background, vegetation cover in the region was high. Seasonal floods carried large volumes of clastic material, leading to rapid accumulation, frequent channel avulsion, and anabranching, forming broad and shallow braided channels. By the upper part of the First Member, seasonal precipitation intensified and evaporation increased, resulting in reduced vegetation cover within the drainage basin. Nevertheless, intermittent rainfall still maintained periodic surface runoff. At this stage, river transport capacity weakened, the proportion of fine-grained sediments increased, and bank resistance to erosion was enhanced by the consolidation of local vegetational debris. Consequently, the lateral migration rate of channels decreased, and meandering rivers began to develop, superimposed upon the earlier braided channels. In this transitional environment, alternating plant debris and purple-red to reddish-brown mudstone drape layers appear in the upper sedimentary succession of the First Member, reflecting a paleoclimatic transition from humid to semi-humid conditions.

By the depositional stage of the Second Member of the Halahatang Formation, the mudstone colors are grayish-black and gray, indicating a shift back to a humid paleoclimate. At this time, fine-grained sediments, together with rising base level, expanded the accommodation space, leading to channel flooding and the accumulation of water in depressions. This ultimately resulted in a coastal-shallow lacustrine environment dominated by fine-grained mudstones and biochemical deposits. This climate-driven shift in sedimentary regime essentially represents a response of paleohydrological conditions to base-level changes: as the climate shifted toward a semi-arid to humid type, the rising base level promoted the transition from braided to meandering rivers. Subsequently, as the climate became humid again and base level continued to rise, the fluvial system disintegrated and was replaced by shallow lake environments, thus effecting the transition from meandering river to shore–shallow lacustrine deposits. The resulting depositional transition from braided to meandering rivers is schematically illustrated in Figure 10.

5.2 Depositional Evolution Model and Geological Implications

Combined with sedimentary facies identification, sandbody distribution analysis and fluvial development investigation, the evolution law of sedimentary systems in the study area was discussed in depth, and the sedimentary evolution model of the Triassic Halahatang Formation was established (Figure 11).

Typical braided river deposits developed in the lower part of the First Member of the Halahatang Formation in the study area. During the early depositional stage, the base level was relatively low, sediment supply was abundant, the topographic slope was steep, and the climate was warm and semi-arid, with seasonal precipitation providing sufficient runoff for braided channel development. The sedimentary facies mainly include underwater distributary channels, interdistributary areas, and underwater interdistributary bays of the braided river delta front.

In the upper part of the First Member, as the base level rose, sediment supply decreased, the topographic slope became gentler, and the climate gradually turned arid, thin-bedded sandbodies exhibit characteristics of few layers (1-2 layers) and small thickness, forming a retrogradational sequence under a relatively high A/S ratio. The braided river channels gradually narrowed and aggraded laterally, forming staggered and laterally composite superposed deposits in a short

Sedimentary Facies / Controlling Factors	Braided River Deposit (Member Ha-1)	Braided-Meandering Transition Deposit (Upper Member Ha-1)	Shore-Shallow Lake Deposit (Member Ha-2)
Base-level Cycle	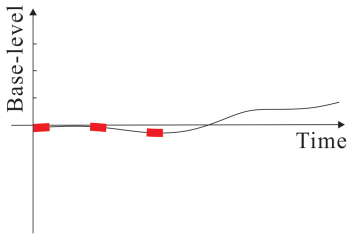	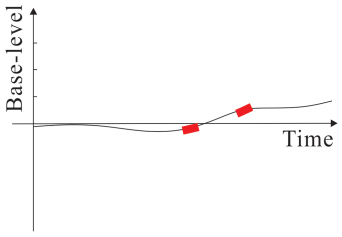	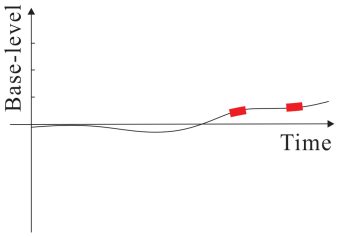
Paleoclimate	Semi-humid Climate	Semi-arid to Humid Climate	Humid Climate
Slope Gradient	Steep Slope	Relatively Gentle Slope	Gentle Slope
Sediment Supply	Strong Sediment Supply from the North	Moderate Sediment Supply	Distal and Weak Sediment Supply
Sand-to-Strata Ratio	70%–80%	30%–45%	15%–25%
Lithofacies Association	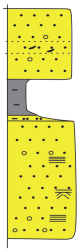	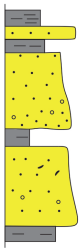	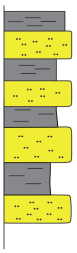

Figure 10. Schematic diagram of the transformation characteristics of braided rivers to meandering rivers in the Halahatang Formation.

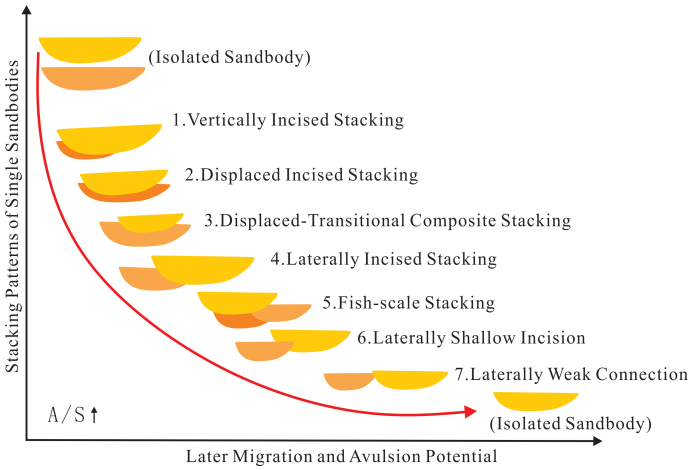

Figure 11. Diagram of sand body slicing and stacking patterns under different A/S controls.

period of time [38]. Such morphological adjustments are consistent with experimental observations demonstrating that reduced sediment supply induces channel narrowing and lateral accretion in sinuous gravel-bed systems [39], with two south-north oriented meandering river channel belts developed.

In the Second Member of the Halahatang Formation, with continuous changes in base level, sediment supply, paleoslope and paleoclimate, the channels gradually transitioned from highly sinuous, laterally migrating meander belts to low-energy, stable distributary networks. Accompanied by weakened fluvial dynamics and periodic flooding of lake water, sedimentation shifted from lateral accretion to vertical accretion-dominated, and the sedimentary environment finally evolved from meandering rivers to shore-shallow lacustrine facies (Figure 12).

6 Conclusions

Integrated analysis of cores, thin sections, well logs, seismic attributes, and well-tie sections indicates

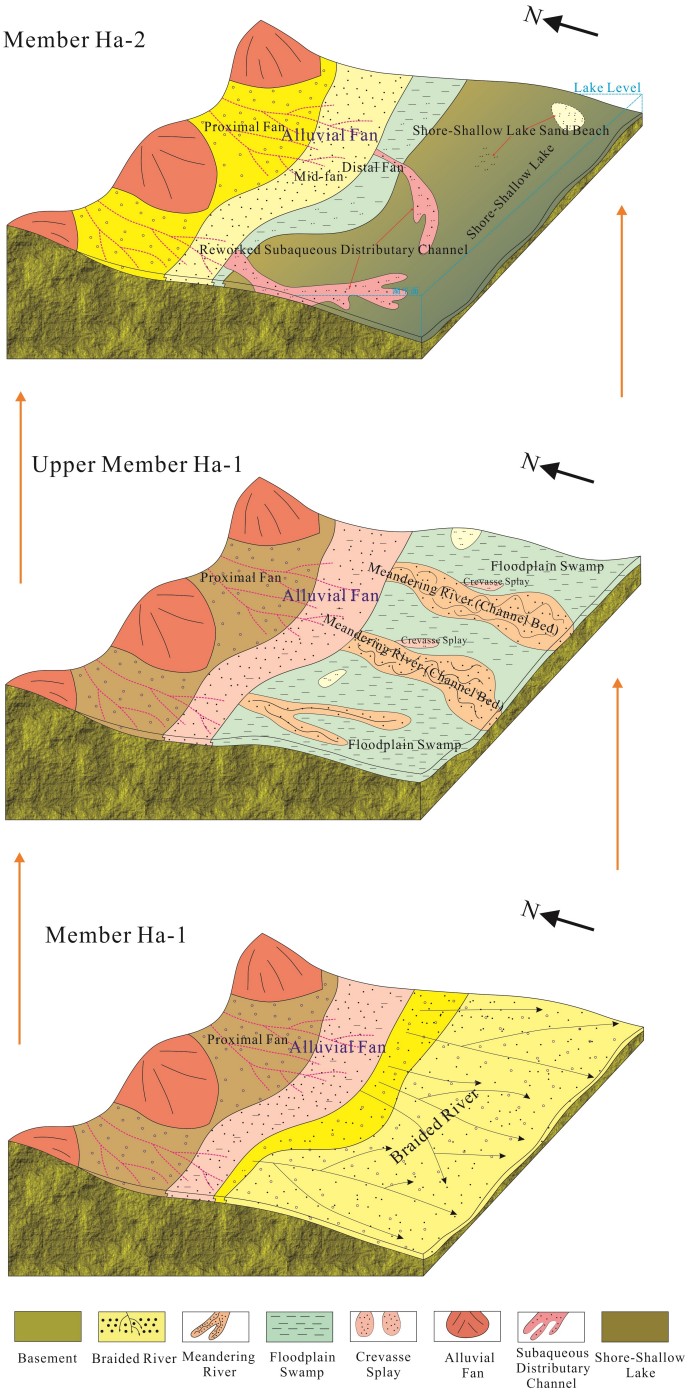

Figure 12. Sedimentary evolution model of the Halahatang Formation.

that the Triassic Halahatang Formation in the Tahe Oilfield comprises ten lithofacies types, including two conglomerate lithofacies, six sandstone lithofacies, and two mudstone lithofacies. These lithofacies are grouped into three major depositional systems: braided river deposits in the lower First Member, meandering river deposits in the upper First Member, and shore–shallow lacustrine deposits in the Second Member.

The lower First Member was deposited under conditions of relatively low base level, abundant northern sediment supply, steep paleotopographic slope, and strong hydrodynamic energy. These conditions favored the formation of thick, coarse-grained, vertically stacked braided-channel sandbodies with frequent channel avulsion, amalgamated sandbody stacking, and episodic scour-fill cycles.

The upper First Member records a clear transition from braided river to meandering river deposition. During this stage, base level rose, sediment supply weakened, paleoslope gradient decreased, and the fluvial energy system became progressively more stable. As a result, channel sandbodies became thinner, mud content increased upward, and sandbody stacking changed from vertically incised amalgamation to staggered and laterally composite superposition. Two main meandering channel belts were identified in this interval.

The Second Member represents the final stage of fluvial weakening and lacustrine expansion. Continued base-level rise and reduced sediment input promoted the development of shore–shallow lacustrine facies, characterized by mud-rich deposits, locally developed sand bars and sand flats, and relatively continuous thin sandbodies. This stage reflects the transformation from channel-dominated fluvial sedimentation to wave- and lake-controlled shallow lacustrine deposition.

The sedimentary evolution of the Halahatang Formation was jointly controlled by base-level change, sediment supply, paleotopographic slope, and paleoclimate. Among these factors, rising base level and decreasing sediment supply played direct roles in reducing channel energy and sandbody amalgamation, whereas paleoslope reduction and climatic fluctuation further promoted the transition from braided to meandering river systems. The established fluvial–lacustrine depositional evolution model provides a practical basis for predicting favorable reservoir sandbodies in the Triassic clastic succession of the Tahe Oilfield.

Data Availability Statement

Data will be made available on request.

Funding

This work was supported by the Major Pilot Project of Sinopec: Hydrocarbon Accumulation Rules and

Key Exploration Technologies in Clastic Strata of Midwestern Basins under Grant 2016KTXD02.

Conflicts of Interest

Hongtao Ma, Wenpin Li, Xindong Diao, Weili Gu are affiliated with the Research Institute of Exploration and Development, Northwest Oilfield Company, Sinopec, Urumqi 830011, China. The authors declare that this affiliation had no influence on the study design, data collection, analysis, interpretation, or the decision to publish, and that no other competing interests exist.

AI Use Statement

The authors declare that no generative AI was used in the preparation of this manuscript.

Ethical Approval and Consent to Participate

Not applicable.

References

[1] Xu, H., Guo, X., Cao, Z., Alves, T. M., Tao, Z., Wang, B., ... & Luo, T. (2025). Petroleum-charge history of Paleozoic carbonates in the Tahe oil field, Tarim Basin, northwestern China: Insights from oil geochemistry, fluid inclusion, and U-Pb dating. *AAPG Bulletin, 109*(1), 57-84. [CrossRef]

[2] Miall, A. D. (2013). *The geology of fluvial deposits: sedimentary facies, basin analysis, and petroleum geology*. Springer. [CrossRef]

[3] Liu, Z., Yu, Y., Wang, L., Wu, H., & Lin, Q. (2025). Sedimentary characteristics of the sandstone intervals in the fourth member of Triassic akekule formation, Tarim basin: Implications for petroleum exploration. *Applied Sciences, 15*(6), 3297. [CrossRef]

[4] Wu, H., Cheng, X., Chen, H., Chen, C., Dilek, Y., Shi, J., ... & Zhang, F. (2021). Tectonic switch from Triassic contraction to Jurassic-Cretaceous extension in the western Tarim Basin, Northwest China: New insights into the evolution of the Paleo-Tethyan orogenic belt. *Frontiers in Earth Science, 9*, 636383. [CrossRef]

[5] Jolivet, M., Dominguez, S., Charreau, J., Chen, Y., Li, Y., & Wang, Q. (2010). Mesozoic and Cenozoic tectonic history of the central Chinese Tian Shan: Reactivated tectonic structures and active deformation. *Tectonics, 29*(6). [CrossRef]

[6] Metcalfe, I. (2013). Gondwana dispersion and Asian accretion: Tectonic and palaeogeographic evolution of eastern Tethys. *Journal of Asian Earth Sciences, 66*, 1-33. [CrossRef]

[7] Olsen, H. (1988). The architecture of a sandy braided-meandering river system: an example from the lower triassic Soiling Formation (M. Buntsandstein) in W-Germany. *Geologische Rundschau, 77*(3), 797-814. [CrossRef]

[8] Kasse, C., Van Balen, R. T., Bohncke, S. J. P., Wallinga, J., & Vreugdenhil, M. (2017). Climate and base-level controlled fluvial system change and incision during the last glacial–interglacial transition, Roer river, the Netherlands–western Germany. *Netherlands Journal of Geosciences, 96*(2), 71-92. [CrossRef]

[9] Sharma, N., Whittaker, A. C., Watkins, S. E., Valero, L., Vérité, J., Puigdefabregas, C., ... & Castelltort, S. (2023). Water discharge variations control fluvial stratigraphic architecture in the Middle Eocene Escanilla formation, Spain. *Scientific Reports, 13*(1), 6834. [CrossRef]

[10] Allen, J. P., Fielding, C. R., Gibling, M. R., & Rygel, M. C. (2014). Recognizing products of palaeoclimate fluctuation in the fluvial stratigraphic record: an example from the Pennsylvanian to Lower Permian of Cape Breton Island, Nova Scotia. *Sedimentology, 61*(5), 1332-1381. [CrossRef]

[11] Colombera, L., & Mountney, N. P. (2019). The lithofacies organization of fluvial channel deposits: A meta-analysis of modern rivers. *Sedimentary Geology, 383*, 16-40. [CrossRef]

[12] Makaske, B. (2001). Anastomosing rivers: a review of their classification, origin and sedimentary products. *Earth-Science Reviews, 53*(3-4), 149-196. [CrossRef]

[13] Słowik, M., Dezső, J., Kovács, J., Gałka, M., & Sipos, G. (2022). Conditions to preserve the sedimentary record of channel planforms in temperate rivers of the Northern Hemisphere. *Journal of Geophysical Research: Earth Surface, 127*(3), e2021JF006188. [CrossRef]

[14] Kędzior, A., Widera, M., & Zieliński, T. (2021). Ancient and modern anastomosing rivers: insights from sedimentological and geomorphological case studies of the Triassic, Neogene and Holocene of Poland. *Geological Quarterly, 65*(4), 111-138. https://bibliotekanauki.pl/articles/2058684.pdf

[15] Min, Y. A. N. G., Jinhua, L. I. U., Wei, X. I. A. N., Rui, G. U. O., & Buyu, X. I. A. (2019). Description of the Boundary of Banded Sand Body in the Fourth Member of Akekule Formation in Eastern Tahe Oilfield, Tarim Basin. *Xinjiang Petroleum Geology, 40*(4), 1. http://dianda.cqvip.com/Qikan/Article/Detail?id=7002535190

[16] Laborde, A., Barrier, L., Simoes, M., Li, H., Coudroy, T., van Der Woerd, J., & Tapponnier, P. (2019). Cenozoic deformation of the Tarim Basin and surrounding ranges (Xinjiang, China): A regional overview. *Earth-Science Reviews, 197*, 102891. [CrossRef]

[17] Kaya, M. Y., Dupont-Nivet, G., Proust, J. N., Roperch, P., & Bougeois, L. (2019). Paleogene evolution and demise of the proto-Paratethys Sea in Central Asia (Tarim and Tajik basins): role of intensified tectonic activity at ca. 41 Ma. *Basin Research, 31*(3), 461-486. [CrossRef]

[18] Lin, C., Li, H., & Liu, J. (2012). Major unconformities,

tectonostratigraphic frameword, and evolution of the superimposed Tarim basin, Northwest China. *Journal of Earth Science, 23*(4), 395-407. [CrossRef]

[19] He, B., Jiao, C., Xu, Z., Cai, Z., Zhang, J., Liu, S., ... & Yu, Z. (2016). The paleotectonic and paleogeography reconstructions of the Tarim Basin and its adjacent areas (NW China) during the late Early and Middle Paleozoic. *Gondwana Research, 30*, 191-206. [CrossRef]

[20] Jiang, Z., Jiang, S., Lan, X., Wang, B., Huang, S., & Zhang, H. (2018). Neotectonic evolution of the Tarim Basin Craton from Neogene to quaternary. *International Geology Review, 60*(10), 1213-1230. [CrossRef]

[21] Lin, C., Yang, H., Liu, J., Rui, Z., Cai, Z., & Zhu, Y. (2012). Distribution and erosion of the Paleozoic tectonic unconformities in the Tarim Basin, Northwest China: Significance for the evolution of paleo-uplifts and tectonic geography during deformation. *Journal of Asian Earth Sciences, 46*, 1-19. [CrossRef]

[22] Wang, C., Wu, H., Dilek, Y., Zhang, F., Chen, H., Li, F., ... & Cheng, X. (2025). Multiple episodes of late Neoproterozoic rifting in the Tarim Craton during its separation from the supercontinent Rodinia. *Journal of the Geological Society, 182*(2), jgs2024-076. [CrossRef]

[23] Shuping, C., Yi, W., & Zhijun, J. (2007). Controls of tectonics on both sedimentary sequences and petroleum systems in Tarim Basin, northwest China. *Petroleum Science, 4*(2), 1-9. [CrossRef]

[24] Feng, L., Lu, Y. C., Wellner, J. S., Liu, J. S., Liu, X. F., Li, X. Q., & Zhang, J. Y. (2020). Fluvial morphology and reservoir sand-body architecture in lacustrine rift basins with axial and lateral sediment supplies: Oligocene fluvial–lacustrine succession in the Xihu sag, East China Sea Shelf Basin. *Australian Journal of Earth Sciences, 67*(2), 279-304. [CrossRef]

[25] Wang, J. K., Xia, S. Q., Fan, Q. Q., & Liu, X. L. (2025). The establishment of high-resolution sequence stratigraphy linked to INPEFA analysis in third member of Yanchang Formation, central Ordos Basin. *Applied Geophysics*, 1-13. [CrossRef]

[26] Wu, H., Ji, Y., Wu, C., Duclaux, G., Wu, H., Gao, C., ... & Chang, L. (2019). Stratigraphic response to spatiotemporally varying tectonic forcing in rifted continental basin: Insight from a coupled tectonic-stratigraphic numerical model. *Basin Research, 31*(2), 311-336. [CrossRef]

[27] Ridente, D. (2016). Releasing the sequence stratigraphy paradigm. Overview and perspectives. *Journal of the Geological Society, 173*(5), 845-853. [CrossRef]

[28] Gibling, M. R. (2006). Width and thickness of fluvial channel bodies and valley fills in the geological record: a literature compilation and classification. *Journal of sedimentary Research, 76*(5), 731-770. [CrossRef]

[29] Schumm, S. A. (1985). Patterns of alluvial rivers. *Annual Review of Earth and Planetary Sciences, 13*(1), 5-27. [CrossRef]

[30] Vandenberghe, J. (2001). A typology of Pleistocene cold-based rivers. *Quaternary International, 79*(1), 111-121. [CrossRef]

[31] Li, W. A. N., Xiao-Wei, J. I. A. N. G., & Xu-Sheng, W. A. N. G. (2010). A common regularity of aquifers: The decay in hydraulic conductivity with depth. *Geological Journal of China Universities, 16*(1), 7. https://geology.nju.edu.cn/EN/Y2010/V16/I1/7

[32] Mou, Z. H. (1993). A new method to calculate the ancient thickness of sedimentary sequences. *Experiment Petroleum Geology, 15*(4), 414-422. [CrossRef]

[33] Nichols, G. (2009). *Sedimentology and stratigraphy*. John Wiley & Sons.

[34] Catuneanu, O. (2020). Sequence stratigraphy in the context of the 'modeling revolution'. *Marine and Petroleum Geology, 116*, 104309. [CrossRef]

[35] Peng, J., Li, J., Li, W., Slater, S. M., Zhu, H., & Vajda, V. (2018). The triassic to early jurassic palynological record of the Tarim basin, China. *Palaeobiodiversity and Palaeoenvironments, 98*(1), 7-28. [CrossRef]

[36] Jiang, D. X., Wang, Y. D., Robbins, E. I., Wei, J., & Tian, N. (2008). Mesozoic non-marine petroleum source rocks determined by palynomorphs in the Tarim Basin, Xinjiang, northwestern China. *Geological Magazine, 145*(6), 868-885. [CrossRef]

[37] Bing, H. (1994). Study on triassic fin delta sedimention and reservoir in Lunnan Area Tarim basin. *Acta Sedimentologica Sinica, 12*(2), 54-62. http://www.cjxb.ac.cn/en/article/id/2104

[38] Clift, P. D., Olson, E. D., Lechnowskyj, A., Moran, M. G., Barbato, A., & Lorenzo, J. M. (2019). Grain-size variability within a mega-scale point-bar system, False River, Louisiana. *Sedimentology, 66*(2), 408-434. [CrossRef]

[39] Rachelly, C., Friedl, F., Boes, R. M., & Weitbrecht, V. (2021). Morphological response of channelized, sinuous gravel-bed rivers to sediment replenishment. *Water Resources Research, 57*(6), e2020WR029178. [CrossRef]

Qihang Ren is a Master's candidate at the School of Geoscience and Technology, Southwest Petroleum University, China. His research interests include petroleum geology. (Email: 2410052155@qq.com)

Jinhua Liu is an Associate Professor at the School of Geoscience and Technology, Southwest Petroleum University, China. He received his Ph.D. from China University of Petroleum (East China). His research interests include geoscience engineering and scientific education. (Email: 499504140@qq.com)